



HAL
open science

Substitutional Carbon Incorporation in SiGeC/Si Heterostructures: Influence of Silicon Precursors

Jérémy Vives, Fabien Deprat, Didier Dutartre, Justine Lespiaux, Romain Duru, Mehmet Bicer, Nathalie Drogue, Marc Juhel, Didier Chaussende

► **To cite this version:**

Jérémy Vives, Fabien Deprat, Didier Dutartre, Justine Lespiaux, Romain Duru, et al.. Substitutional Carbon Incorporation in SiGeC/Si Heterostructures: Influence of Silicon Precursors. *ECS Transactions*, 2022, 109 (4), pp.237-248. 10.1149/10904.0237ecst . hal-04042448

HAL Id: hal-04042448

<https://hal.science/hal-04042448>

Submitted on 23 Mar 2023

HAL is a multi-disciplinary open access archive for the deposit and dissemination of scientific research documents, whether they are published or not. The documents may come from teaching and research institutions in France or abroad, or from public or private research centers.

L'archive ouverte pluridisciplinaire **HAL**, est destinée au dépôt et à la diffusion de documents scientifiques de niveau recherche, publiés ou non, émanant des établissements d'enseignement et de recherche français ou étrangers, des laboratoires publics ou privés.

Substitutional Carbon Incorporation in SiGeC/Si Heterostructures: Influence of Silicon Precursors

J. Vives^{a,b}, F. Deprat^a, D. Dutartre^a, J. Lespiaux^a, R. Duru^a, M. Bicer^a, N. Drogue^a, M. Juhel^a, D. Chaussende^b

^a STMicroelectronics, 850 rue Jean Monnet, 38926 Crolles, France

^b Univ. Grenoble Alpes, CNRS, Grenoble INP, SIMaP, 38000 Grenoble, France

In this paper, SiGe or SiGeC epitaxy with Silane or Disilane, Germane and Methylsilane precursors was studied in a 300 mm industrial Reduced Pressure-Chemical Vapor Deposition (RP-CVD) reactor. The SiGe growth rate exponentially increased with the temperature in the 500 °C - 600 °C range for both silicon precursors (activation energy $E_a = 2.1$ eV). It was, at 550 °C, almost twice higher with Si₂H₆ than with SiH₄. At low temperature, Si₂H₆ is indeed more reactive than SiH₄, resulting in SiGe growth rates significantly higher for a given germanium composition. Then, carbon incorporation at 550 °C into Si_{0.8}Ge_{0.2} was studied. The higher reactivity of Si₂H₆ compared to SiH₄ resulted in a better substitutional carbon incorporation. In our experimental conditions, 1.2 at% of fully substitutional carbon atoms could indeed be obtained with Si₂H₆ (without any detectable interstitial ones). Meanwhile, only 0.5 at% of fully substitutional carbon atoms was obtained with SiH₄.

Introduction

The incorporation of germanium and carbon into silicon is very interesting for various types of silicon-based devices because the variety of properties that can be tailored, such as: band gap or lattice parameter engineering, dopant diffusion reduction, chemical properties, optical properties... Hetero-junction Bipolar Transistors, strained channel Complementary Metal Oxide Semiconductor devices, Infra-Red photo-detectors, elevated Sources and Drains, Micro-Electro-Mechanical Systems, virtual substrates for III-V integration and so on benefit from such a tailoring (1).

However, the growth of carbon containing films is quite difficult because of the high mismatch between Si and C lattices (52%), the low bulk solubility of C into Si (10^{-4} at% C at 1400 °C) and an even lower one in Ge (2). Fortunately, during epitaxial growth, carbon incorporation is not critically dependent on the equilibrium bulk solubility, but rather on “surface mechanisms”. Calculations for carbon on a Si(001) surface suggest a solubility enhancement of 10^4 over equilibrium bulk solubility (3).

Non-equilibrium growth methods such as molecular beam epitaxy (MBE) or chemical vapor deposition (CVD) can be used to grow Si_{1-x-y}Ge_xC_y layers with carbon concentrations of several percent. However, in many cases, not all the carbon atoms are located in substitutional sites of the lattice (C_{sub}). Beyond a threshold total carbon concentration (C_{tot}) (depending on process parameters), carbon atoms are also incorporated into interstitial sites

(C_{int}). These C_{int} atoms usually form extended defects such as clusters or SiC precipitates which are harmful for device performances (4). It has been clearly demonstrated that low temperatures and high growth rates are suitable to avoid SiC precipitates and promote C incorporation into substitutional sites (5) (6).

In this paper, the SiGe growth kinetics was investigated at low temperature using SiH_4 and Si_2H_6 as silicon precursors. Then, SiH_4 and Si_2H_6 precursors were compared to obtain at low temperature, thin SiGeC films with the highest amount of C_{sub} without C_{int} .

Experimental details

A 300 mm Epi Centura RP-CVD reactor from Applied Material was used to grow all epitaxial layers, with the pressure chamber fixed at 10 Torr. The purified hydrogen (H_2) carrier gas flow rate, several tens standard liters per minute (slm), was also fixed throughout the experiments. Pure Silane (SiH_4) and Disilane (Si_2H_6) were used as Si precursors. Germane (GeH_4) and Methylsilane (SiH_3CH_3) diluted at 1.5% and 2% in H_2 , respectively, were used as Ge and C sources. All layers were grown on slightly p-type doped 300 mm Si(001) blanket wafers. Prior to epitaxy, an in-situ H_2 annealing at 1050 °C during 90s was performed to remove the 10 Å thick chemical oxide present on the surface of wafers.

SiGe and SiGeC growth rates were determined through thickness measurements with X-Ray reflectivity (XRR). Conventional omega-2theta scans around the (004) X-ray diffraction (XRD) peak were used to check that layers were of high crystalline quality, to determine the Ge concentrations in SiGe layers and the “apparent” Ge concentrations in SiGeC layers. In our industrial XRD setup, profile acquisition uses a convergent beam over four degrees combined to a linear detector in a two-step process. A first fast acquisition was performed to find the Si substrate peak and set its angular position to 0°. In a second acquisition, the Si peak was removed (angles -0.15° and above) with a narrow slit before the detector so that the scan only includes the intensity diffracted from the active layer and not that from the substrate. This strategy helps to improve the signal/noise ratio of the layer, which is particularly beneficial to the acquisition of SiGe and SiGeC diffraction fringes in the vicinity of the Si substrate peak. XRD profiles in the following will thus show the intensities of diffracted X-rays as functions of their angular offset with the Si (004) substrate peak used for reference. The downside is that some of layer’s peaks (especially for high SiH_3CH_3 mass flows and thus reduced compressive strains) might seem deformed without any thickness fringes at high incidence angles. XRD and XRR measurements were performed on the same Jordan-Valley JVX7300 tool.

Secondary Ions Mass Spectrometry (SIMS) using Cs^+ primary ions, with an impact energy of 1 keV, was used for the depth profiling of the atomic Si, Ge and C concentrations in SiGe and SiGeC layers. SIMS measurements gave access to atomic (i.e real) Ge and C concentrations. C atomic concentrations C_{tot} were determined thanks to carbon implanted SiGe reference samples. Fourier Transform Infrared Spectroscopy (FTIR) measurements were carried out in a Onto QS-3300 tool to check whether or not C atoms were in substitutional sites or in configurations close to that to amorphous SiC clusters. Finally, Atomic Force Microscopy (AFM) measurements were performed to have access to the surface morphology of SiGe and SiGeC layers.

SiGe growth kinetics with Silane (SiH₄) and Disilane (Si₂H₆)

Evolution with temperature of the growth kinetics of intrinsic SiGe

The SiGe growth rates at 10 Torr with constant Si and Ge flows are plotted as functions of the reverse absolute temperature in **Figure 1a**.

To have the same flows of Si, the disilane mass flow was set to half that of silane, as there are two Si atoms in a Si₂H₆ molecule instead of one in a SiH₄ one (i.e. $F(\text{Si}_2\text{H}_6)/F(\text{H}_2) = 0.0015$ and $F(\text{SiH}_4)/F(\text{H}_2) = 0.003$). Over the entire range of temperatures, the SiGe growth rate was higher with Si₂H₆ than with SiH₄, this for the same flows of Si atoms. It was for instance 1.85 times higher at 550 °C.

We otherwise had, for both precursors, the usual exponential increase of the SiGe growth rate with the temperature in the 500 °C – 600 °C range. The activation energies ($E_a = 2.06$ and $E_a = 2.09$ eV for SiH₄ and Si₂H₆, respectively), were identical, suggesting that growth limiting mechanisms were similar. It was most likely H-desorption from Si sites ($E_d = 2$ eV) instead of that from Ge sites ($E_d = 1.6$ eV) that governed such an increase (7) (8).

Figure 1b shows the evolutions of the Ge concentration in SiGe alloys as a function of the temperature. The Ge concentration was lower with Si₂H₆ than SiH₄. In both cases, the Ge content decreased as the temperature increased.

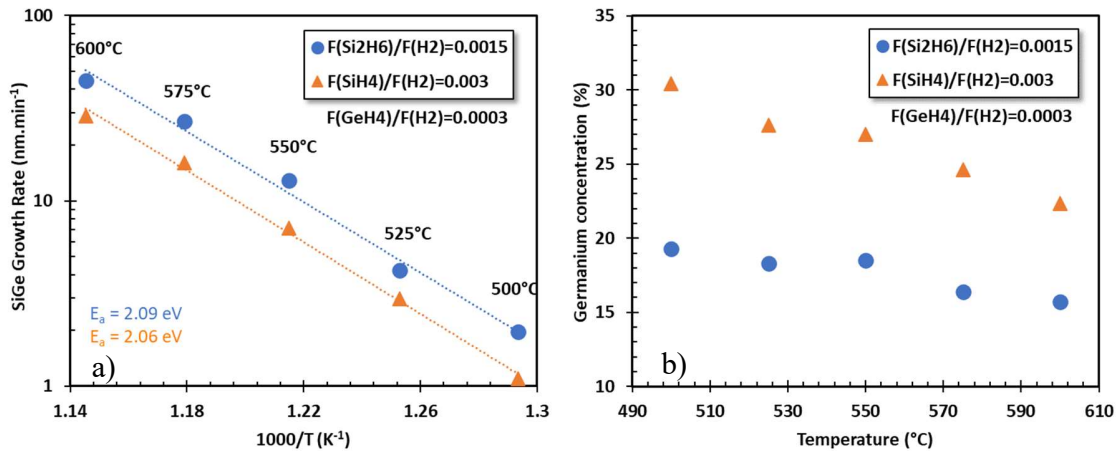


Figure 1. SiGe growth rate at 10 Torr as a function of the reverse absolute temperature (a) and associated Ge content as a function this time of the temperature (b). The atomic flow of Si was the same ($F(\text{Si}_2\text{H}_6)/F(\text{H}_2) = 0.0015$ and $F(\text{SiH}_4)/F(\text{H}_2) = 0.003$). The GeH₄ mass flow was fixed at $F(\text{GeH}_4)/F(\text{H}_2) = 0.0003$.

To have a better understanding of such growth kinetics differences, an impoverishment rate of gaseous reactive species was calculated. It was the ratio between the number of moles of Si (or Ge) deposited per minute ($n_{\text{deposited}}$) (*2 in the case of Si₂H₆ as there are two Si atoms in this molecule) and the number of moles of silicon precursor (or germanium) injected (n_{injected}) into the epitaxy reactor per minute:

$$\alpha_{precursor} = \frac{n_{deposited}}{n_{injected}} = \frac{GR * S * \rho_{Si(or Ge)} * X_{Si(or Ge)} * V^{\circ}}{M_{Si(or Ge)} * d_{precursor}} \quad [1]$$

Where GR is the growth rate (cm.min⁻¹), S the deposition surface (cm²), ρ the Si (or Ge) density (g.cm⁻³), x the Si (or Ge) molar fraction, V° the molar volume under standard conditions of temperature and pressure (cm³.mol⁻¹), M the Si (or Ge) molar mass (g.mol⁻¹) and $d_{precursor}$ the Si precursor (or GeH₄) mass flow (cm³.min⁻¹). However, there are some incertitudes about the absolute values of impoverishment rates. Indeed, in RP-CVD, there is a deposition not only on the wafer but also, for example, on the quartz domes, the susceptor plate, the outer ring and so on. For these calculations, we thus assumed that the deposition surface was that of the susceptor plate and the outer ring, i.e. 2026 cm².

Impoverishment rates of silicon precursors (a) and GeH₄ (b) are plotted in **Figure 2**.

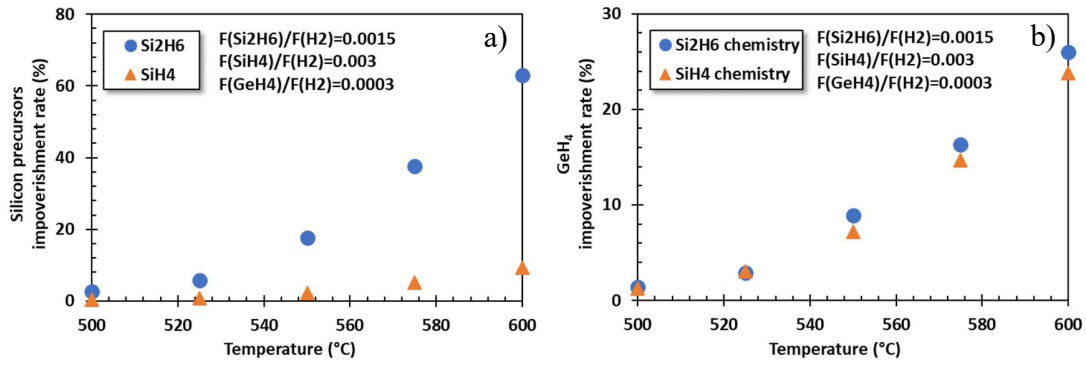


Figure 2. Silicon precursors (a) and GeH₄ (b) impoverishment rates as functions of the temperature.

Figure 2a shows that the impoverishment rate of the Si₂H₆ precursor increases faster than the SiH₄ one as the epitaxy temperature increases. Si₂H₆ molecules are decomposed more than SiH₄ ones, which is a very clear sign of a difference in reactivity between those precursors. This result was expected, as the Si-Si bond strength (226 kJ.mol⁻¹) is weaker than the Si-H bond strength (318 kJ.mol⁻¹) (9). Consequently, the chemical decomposition of the silicon precursor and the formation of hydrogenated Si sub-species are easier with Si₂H₆ than SiH₄.

The GeH₄ impoverishment rate is plotted in **Figure 2b**. GeH₄ impoverishment rates are almost identical for both silicon precursors over the entire temperature range. We can thus suppose that the lower Ge concentration with Si₂H₆ noticed in Figure 1b is due to a higher reactivity of Si₂H₆ compared to SiH₄ (for a given atomic Si flow), resulting in a higher Si growth rate component.

Impact of GeH₄ mass flow on the SiGe growth kinetics

The SiGe growth rate (a) and the germanium content (b) at 550 °C, 10 Torr, are plotted in **Figure 3** as functions of the F(GeH₄)/F(H₂) ratio.

The SiGe growth rate increase when adding larger amounts of GeH₄ (**Figure 3a**) is explained by the fact that Ge atoms act as desorption centers (10), lowering the activation

energy for H-desorption, which is the rate limiting step. Consequently, more nucleation sites are available for the adsorption of Si and Ge atoms. An increase of the number of Ge atoms also result in a sublinear increase of the Ge concentration x into $\text{Si}_{1-x}\text{Ge}_x$ alloys (Figure 3b).

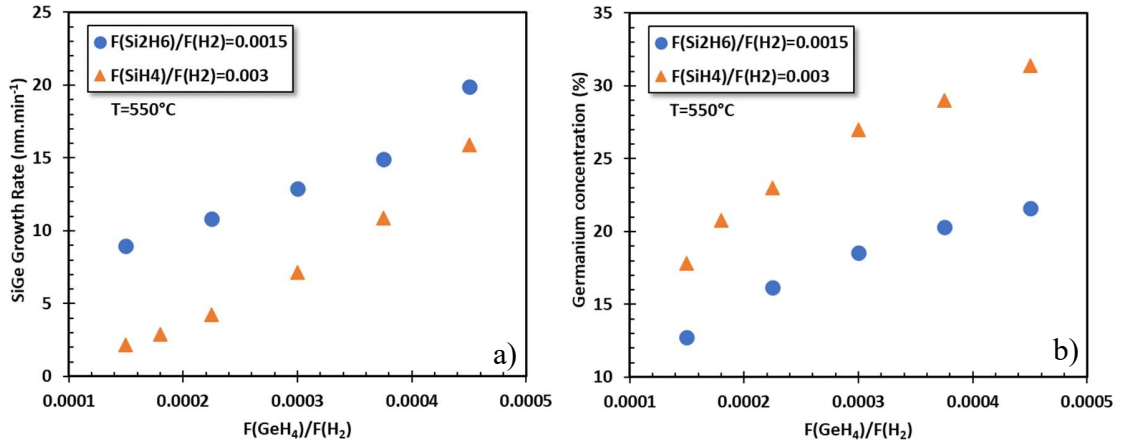


Figure 3. SiGe growth rates (a) and Ge composition (b) at 550 °C, 10 Torr, as functions of the $F(\text{GeH}_4)/F(\text{H}_2)$ ratio.

The Ge content x in $\text{Si}_{1-x}\text{Ge}_x$ can be described with the following relationship derived from the theoretical model proposed by Robbins et al. (8) ($F(\text{Si}) = F(\text{SiH}_4)$ or $2 \cdot F(\text{Si}_2\text{H}_6)$):

$$\frac{x^{n+1}}{1-x} = m * \frac{F_{\text{GeH}_4}}{F_{\text{Si}}} \quad [2]$$

m being a constant depending on the experimental conditions.

The dependency of the Ge concentration x on the $F(\text{GeH}_4)/[F(\text{SiH}_4)$ or $2 \cdot F(\text{Si}_2\text{H}_6)]$ mass flow ratio (MFR) is almost linear for a SiH_4 -based chemistry (Figure 4).

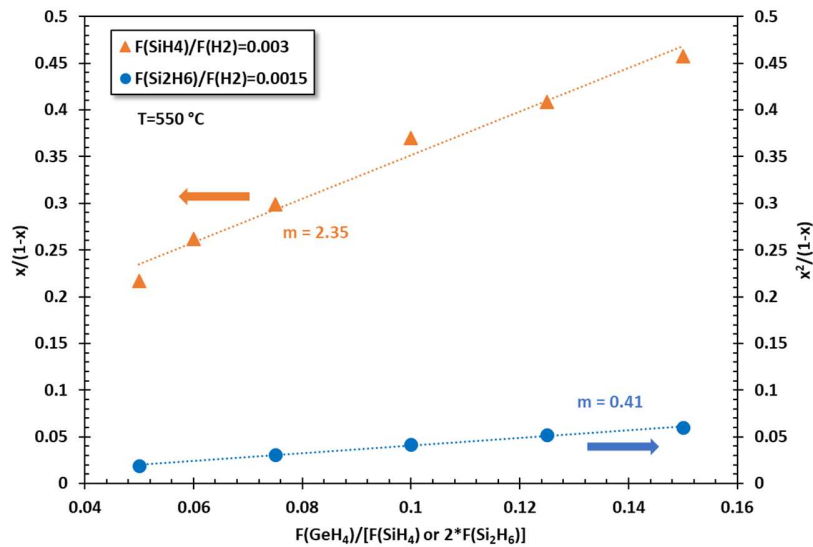


Figure 4. Dependency of $x/(1-x)$ or $x^2/(1-x)$ on the $F(\text{GeH}_4)/F(\text{Si})$ MFR at 550 °C, 10 Torr.

The fit is good with a $x/(1-x)=m*(F(\text{GeH}_4)/F(\text{SiH}_4))$ relationship, with m equal to 2.35. However, the x dependency on the $F(\text{GeH}_4)/F(\text{Si})$ MFR is parabolic-like for a Si_2H_6 -based chemistry. It is well accounted for with a $x^2/(1-x)=m*(F(\text{GeH}_4)/2*F(\text{Si}_2\text{H}_6))$ relationship, with $m = 0.41$.

Such trends and m values are in rather good agreement with some work at higher pressure in another brand of RP-CVD tools (9) ($m = 2.61$ (instead of 2.35 here) and 0.47 (instead of 0.41 here) for SiH_4 and Si_2H_6 at 550 °C, 20 Torr).

The over-linear increase of SiGe growth rate with the Ge content is plotted in **Figure 5** for both chemistries.

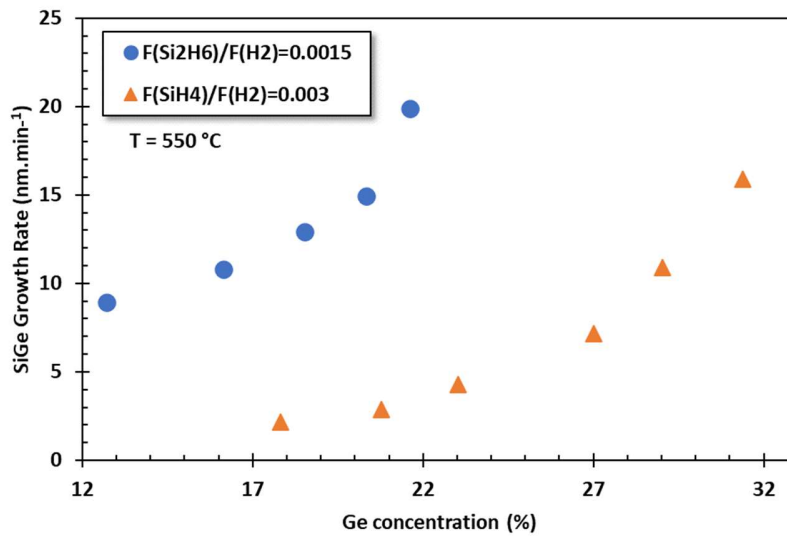


Figure 5. SiGe growth rates at 550 °C, 10 Torr, as a function of the Ge content.

Due to the higher reactivity of Si_2H_6 compared to SiH_4 , SiGe growth rates are significantly higher, for a given Ge composition, with Si_2H_6 than with SiH_4 .

At 550 °C, 10 Torr, Si_2H_6 is a silicon precursor delivering higher growth rates (8.9 - 19.9 $\text{nm}\cdot\text{min}^{-1}$) for low Ge contents (between 12.7 and 21.6%). Meanwhile, SiH_4 is more appropriate for high Ge contents (between 17.8 and 31.4%) with growth rates between 2.16 and 15.9 $\text{nm}\cdot\text{min}^{-1}$.

Carbon incorporation into $\text{Si}_{0.8}\text{Ge}_{0.2}$ with SiH_4 and Si_2H_6

Impact of SiH_3CH_3 mass flow on the SiGeC growth rate

C incorporation into $\text{Si}_{0.8}\text{Ge}_{0.2}$ was investigated at 550 °C, 10 Torr. GeH_4 mass flows were then constant and such that $F(\text{GeH}_4)/F(\text{H}_2) = 0.000375$ for Si_2H_6 and $F(\text{GeH}_4)/F(\text{H}_2) = 0.00018$ for SiH_4 . This resulted in $\text{Si}_{0.8}\text{Ge}_{0.2}$ growth rates of 2.9 and 14.1 $\text{nm}\cdot\text{min}^{-1}$ with SiH_4 and Si_2H_6 , respectively.

The growth rates of SiGeC epitaxial layers are plotted in **Figure 6** as functions of the $F(\text{SiH}_3\text{CH}_3)/[F(\text{GeH}_4) + F(\text{SiH}_4) \text{ or } 2*F(\text{Si}_2\text{H}_6)]$ mass flow ratio (SiH_3CH_3 MFR). The SiGeC growth rate was slightly lower than that of SiGe and monotonously decreased as

the SiH_3CH_3 MFR increased. This was likely due to stronger C-H bonds (80 kcal.mol^{-1}) than Si-H and Ge-H bonds (77.6 and $68.7 \text{ kcal.mol}^{-1}$) impeding H desorption from the growing surface (11).

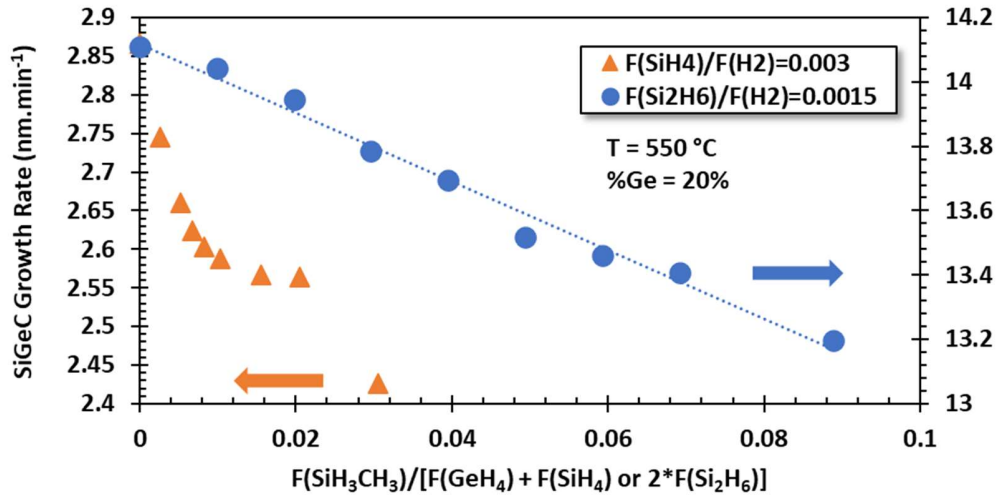


Figure 6. SiGeC growth rates at $550 \text{ }^\circ\text{C}$, 10 Torr, as functions of the $\text{SiH}_3\text{CH}_3/[\text{F}(\text{GeH}_4) + \text{F}(\text{SiH}_4) \text{ or } 2*\text{F}(\text{Si}_2\text{H}_6)]$ MFR. The Ge content was equal to 20 % for both silicon precursors.

However, two trends can be noticed. With Si_2H_6 as the silicon precursor, there is a linear decrease of the growth rate with the SiH_3CH_3 MFR. With SiH_4 , there is at first a sharper decrease, followed by a growth rate plateau then a break. This is likely due to a morphological degradation of the SiGeC layer when the amount of carbon is too high. The SiGeC layer grown with SiH_4 and the highest SiH_3CH_3 MFR is really rough, as shown in **Figure 7**.

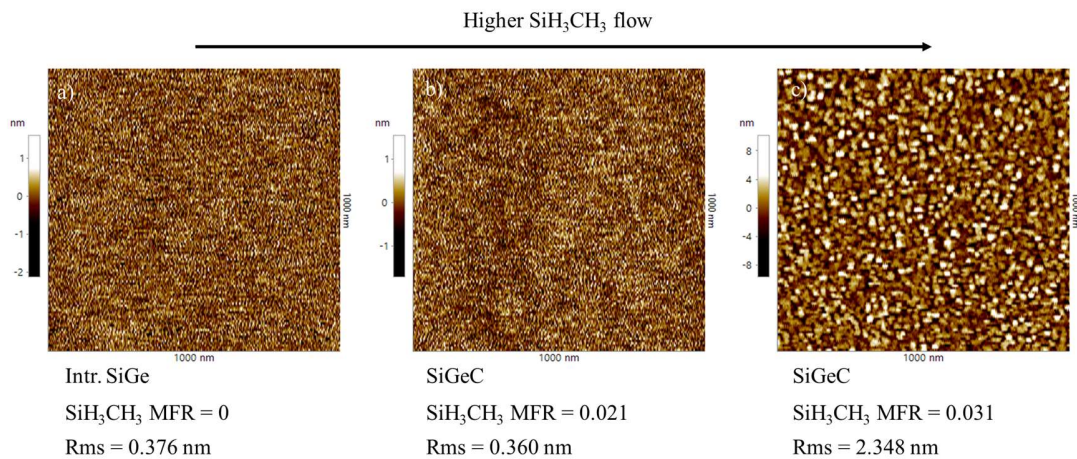


Figure 7. $1\ \mu\text{m} \times 1\ \mu\text{m}$ AFM images of the surface of the intrinsic SiGe (a) and the two SiGeC layers (b) (c) grown with SiH_4 and the highest two SiH_3CH_3 MFRs. The Root mean square (Rms) roughness is provided below each image.

Substitutional and total carbon

XRD has been used to gain access to the “apparent” Ge concentration in SiGeC layers. (**Figure 8**). C atoms, much smaller than Si and Ge atoms ($r_{\text{Si}} = 1.17 \text{ \AA}$, $r_{\text{Ge}} = 1.22 \text{ \AA}$, $r_{\text{C}} = 0.77 \text{ \AA}$) (12), will compensate the compressive strain induced by Ge in SiGe epitaxial layers. It will reduce the out-of-plane lattice parameter and thus yield smaller Ge concentrations, in XRD, than the real Ge concentration (hence the term “apparent”).

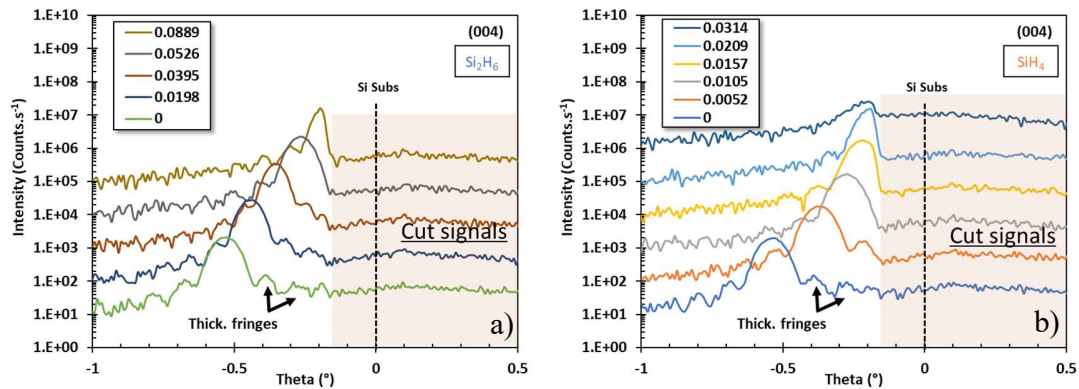


Figure 8. ω - 2θ scans around the (004) diffraction peak associated to some of the SiGe and SiGeC layers grown at 550 °C, 10 Torr with Si_2H_6 (a) and SiH_4 (b). The SiH_3CH_3 MFRs are given in the inset. XRD profiles have been shifted vertically for clarity.

The presence of well-defined and intense layer peaks with thickness fringes on both sides is characteristic of high structural quality SiGeC layers. However, a very weak signal with no thickness fringes is observed for the SiGeC layer grown with SiH_4 and the highest SiH_3CH_3 MFR. This is linked to the crystalline quality degradation and surface roughening for that layer shown in Figure 7. The higher the SiH_3CH_3 MFR is, the more the layer peak shifts towards higher incidence angles, indicating that the distance between (004) lattice planes decreases and that the magnitude of compressive strain decreases. This clearly illustrates the strain compensation by carbon atoms in SiGeC epitaxial films.

A carbon free SiGe sample was used as a reference to calculate the substitutional carbon concentration in SiGeC films. We indeed assumed that C and Ge atoms are independently incorporated (13) and thus that all the SiGeC samples had the same Ge content than the reference film.

Several Ge:C strain compensation ratios for $\text{Si}_{1-x-y}\text{Ge}_x\text{C}_y$ ternary alloys have been reported in the literature (**Table 1**). a_{Si} , a_{Ge} , a_{SiC} , a_{C} are the Si, Ge, SiC and C lattice parameters, respectively. x and y are the concentration of Ge and C, respectively. In our study, a Ge:C strain compensation ratio of 11.75 was used, meaning that 1 at % of C_{sub} atoms compensated the compressive strain coming from 11.75 % Ge in $\text{Si}_{1-x-y}\text{Ge}_x\text{C}_y$.

TABLE 1. Strain compensation ratios in the literature for $\text{Si}_{1-x-y}\text{Ge}_x\text{C}_y$ ternary alloys.

References	$\text{Si}_{1-x-y}\text{Ge}_x\text{C}_y$ lattice parameter	Ge:C strain compensation ratio
Regolini (14)	$a_{\text{Si}}(1-x-y) + a_{\text{Ge}}x + a_{\text{C}}y$	8.2:1
Osten (15)	$a_{\text{Si}}(1-x-2y) + a_{\text{Ge}}x + 2a_{\text{Si}}cy$	10:1
This work	$a_{\text{Si}}(1-x-y) + a_{\text{Ge}}x + a_{\text{C}}y - 0.0272x(1-x) - 0.5705y(1-y)$	11.75:1
De Salvador (16)	$a_{\text{Si}}(1-x-y) + a_{\text{Ge}}x + a_{\text{C}}y - 0.026x(1-x) - 0.59y(1-y) + 0.06xy$	12:1
Windl (17)	-	$15 \pm 3:1$

The total C concentrations (C_{tot}) from SIMS, are plotted in **Figure 9** together with C_{sub} from XRD, as functions of the SiH_3CH_3 MFRs. C_{tot} increases linearly with the SiH_3CH_3 MFR whatever the silicon precursor. With Si_2H_6 , C_{sub} and C_{tot} values are in good agreement, meaning that all carbon atoms are in substitutional sites. With our experimental conditions, we succeeded in having 1.2% of fully substitutional carbon into $\text{Si}_{0.8}\text{Ge}_{0.2}$ layers grown at 550°C , 10 Torr with Si_2H_6 .

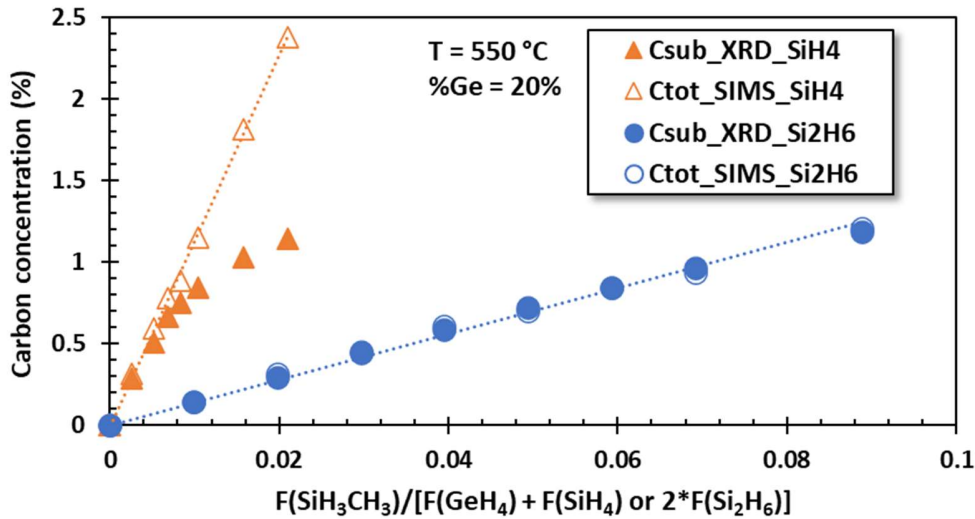


Figure 9. C concentrations (C_{sub} from XRD and C_{tot} from SIMS) in $\text{Si}_{1-0.8-y}\text{Ge}_{0.2}\text{C}_y$ layers grown at 550°C , 10 Torr as functions of the $\text{SiH}_3\text{CH}_3/[\text{F}(\text{GeH}_4) + \text{F}(\text{SiH}_4) \text{ or } 2*\text{F}(\text{Si}_2\text{H}_6)]$ MFR.

However, another trend is observed with SiH_4 . C_{sub} and C_{tot} values are in good agreement for small C concentrations ($< 0.5\%$ C_{tot}) but a further increase of the SiH_3CH_3 MFR results in a growing divergence between C_{sub} and C_{tot} . This is due to an increase of the number of C atoms in interstitial sites, as the total amount of C atoms (substitutional plus interstitial) increases linearly with the SiH_3CH_3 MFR.

Moreover, Fourier Transform Infrared Spectroscopy (FTIR) was performed to check whether or not C atoms were in substitutional sites or in a configuration close to that of an amorphous SiC cluster. The absorbance curves of $\text{Si}_{0.788}\text{Ge}_{0.2}\text{C}_{0.012}$ and $\text{Si}_{0.776}\text{Ge}_{0.2}\text{C}_{0.024}$ layers grown using Si_2H_6 and SiH_4 , respectively, are plotted in **Figure 10**. The layer grown with Si_2H_6 and therefore 1.2% C_{tot} (equal to C_{sub}) shows only one peak at 605 cm^{-1} ,

corresponding to the substitutional carbon local mode $^{12}\text{C}_{\text{sub}}$ in silicon (18). This confirms results shown in Figure 9, i.e. that all C atoms are in substitutional position.

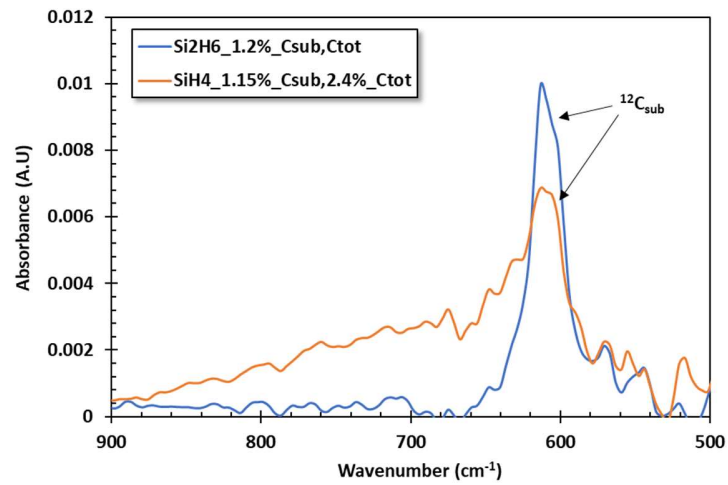


Figure 10. FTIR absorption spectra of $\text{Si}_{0.788}\text{Ge}_{0.2}\text{C}_{0.012}$ and $\text{Si}_{0.776}\text{Ge}_{0.2}\text{C}_{0.024}$ layers using Si_2H_6 and SiH_4 , respectively.

Meanwhile, the absorption curve of the $\text{Si}_{0.776}\text{Ge}_{0.2}\text{C}_{0.024}$ layer (with a C_{sub} of 1.15%) grown using SiH_4 exhibits another absorption band. The broader $^{12}\text{C}_{\text{sub}}$ peak and the presence of an absorption band between 700 and 800 cm^{-1} indicate that only a fraction of the C atoms are in substitutional sites whereas the excess C atoms are in interstitial sites or in a configuration close to that of amorphous SiC clusters (19).

Finally, the C_{tot} dependency on the SiH_3CH_3 MFR can also be described by a simple function as for the Ge concentration (**Figure 11**).

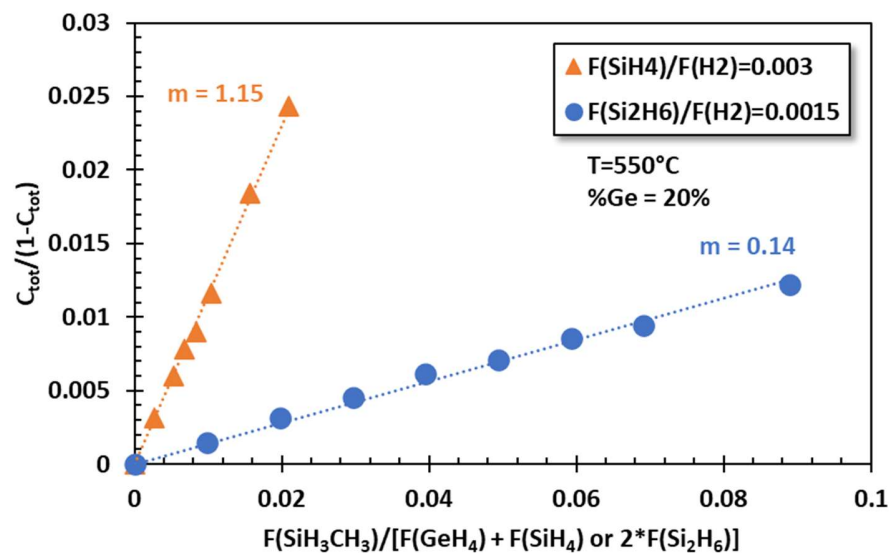


Figure 11. Dependency of $C_{\text{tot}}/(1-C_{\text{tot}})$ on the $\text{SiH}_3\text{CH}_3/[\text{F}(\text{GeH}_4) + \text{F}(\text{SiH}_4) \text{ or } 2*\text{F}(\text{Si}_2\text{H}_6)]$ MFR at 550 °C, 10 Torr.

With SiH₄, m is equal to 1.15, a value in good agreement with previous works (1.11 for a Si_{0.21}Ge_{0.19} layer at 550 °C, 20 Torr) (5). For Si₂H₆, surprisingly, the dependency of C_{tot} on the $F(\text{SiH}_3\text{CH}_3)/(F(\text{GeH}_4)+2*F(\text{Si}_2\text{H}_6))$ MFR is not parabolic (as for the dependency of the Ge content x) but almost linear, with m equal to 0.14. This trend has been observed in (20) with $m = 0.09$ for Si_{1-y}C_y layers at 550 °C, 20 Torr.

Conclusion

In this paper, the low temperature epitaxial growth of SiGe and SiGeC with SiH₄, Si₂H₆, GeH₄ and SiH₃CH₃ as gaseous precursors has been studied in a 300 mm industrial Reduced Pressure-Chemical Vapor Deposition reactor. Si₂H₆, due to the presence of Si-Si bonds (which are weaker than Si-H bonds) was more reactive than SiH₄. Therefore, hydrogenated Si sub-species were more easily available with Si₂H₆ than with SiH₄. Thus, for given GeH₄ and Si precursor mass flow ratios, significantly higher growth rates and lower Ge concentrations were obtained at 550 °C, 10 Torr with Si₂H₆ than with SiH₄. The dependency of the Ge content x on the $F(\text{GeH}_4)/[F(\text{SiH}_4) \text{ or } 2*F(\text{Si}_2\text{H}_6)]$ mass flow ratio, almost linear for SiH₄-based chemistry ($x/(1-x)=2.35*(F(\text{GeH}_4)/F(\text{SiH}_4))$), was parabolic for Si₂H₆-based chemistry ($x^2/(1-x)=0.41*(F(\text{GeH}_4)/2*F(\text{Si}_2\text{H}_6))$).

Then, C incorporation into Si_{0.8}Ge_{0.2} was investigated at 550 °C, 10 Torr. The Si_{0.8}Ge_{0.2} growth rate was almost five times higher with Si₂H₆ than with SiH₄. With Si₂H₆ as a silicon precursor, a linear decrease of the SiGeC growth rate with the SiH₃CH₃ flow was noticed. It was likely due to the introduction of stronger and thus harder to break C-H bonds than Si-H and Ge-H bonds. Meanwhile, a sharper growth rate decrease was evidenced with SiH₄, followed by a growth rate plateau then a drop. This was due to a morphological degradation of the SiGeC layer when the C content was too high.

With Si₂H₆, C_{sub} and C_{tot} concentrations coming from XRD and SIMS were in close agreement over the entire range of SiH₃CH₃ MFR probed. It meant that all C atoms were in substitutional sites, as confirmed by FTIR measurements. In our experimental conditions, we succeeded in having 1.2% of substitutional carbon in a Si_{0.8}Ge_{0.2} layer, without any detectable interstitial carbons.

With SiH₄, C_{sub} and C_{tot} values were in good agreement for small C concentrations (< 0.5 % C_{tot}). For higher C contents, the C_{tot} concentrations continued to increase linearly with the SiH₃CH₃ MFR while the C_{sub} concentration saturated. This showed that a growing fraction of C atoms were incorporated into interstitial sites.

The Si₂H₆ precursor, due to its higher reactivity compared to SiH₄, thus seems to be a better candidate to grow SiGeC layers at low temperature with high growth rates. Consequently, higher concentrations of fully substitutional carbon atoms can be reached with Si₂H₆.

References

1. D. Dutartre, *ECS Trans.* 75 (8) 303-323 (2016).
2. R. W. Olesinski and G. J. Abbaschian, *Bull. Alloy Phase Diagrams* 5, 484 (1984).
3. J. Tersoff, *Phys. Rev. Lett.* 74, 5080 (1995).
4. J. B. Posthill, R. A. Rudder, S. V. Hattangady, G. G. Fountain, and R. J. Markunas, *Appl. Phys. Lett.* 56, 734 (1990).
5. V. Loup, J. M. Hartmann, G. Rolland, P. Holliger, F. Laugier, and M. N. Semeria, *J. Vac. Sci. Technol. B* 21(1), Jan/Feb (2003).
6. H. J. Osten, M. Kim, K. Pressel, and P. Zaumseil, *J. Appl. Phys.* 80 (12), 15 December (1996).
7. M. Hierlemann, A. Kersch, C. Werner, and H. Schäfer, *J. Electrochem. Soc.*, Vol 142, No. 1, January (1995).
8. D. J. Robbins, J. L. Gasper, A. G. Cullis, and W. Y. Leong, *J. Appl. Phys.* 69 (6), 15 March (1991).
9. J. M. Hartmann, V. Benevent, J. F. Damlencourt, and T. Billon, *Thin Solid Films* 520, 3185–3189 (2012).
10. B. Meyerson, K. Uram, F. Legoues, *Appl. Phys. Lett.* 53, 2555 (1988).
11. H. W. Kim, S. Choi, S. Hong, H. K. Jung, G. D. Lee, and E. Yoon, *Journal of the Korean Physical Society*, Vol. 50, No. 3, March (2007).
12. H. J. Osten, M. Kim, G. Lippert, P. Zaumseil, *Thin Solid Films* 294, 93-97 (1997).
13. J. Mi, P. Warren, P. Letourneau, M. Judelewicz, M. Gailhanou, and M. Dutoit, *Appl. Phys. Lett.*, Vol. 67, No. 2, 10 July (1995).
14. J. L. Regolini, F. Gisbert, G. Dolino, and P. Boucaud, *Materials Letters* 18 57-60 (1993).
15. H. J. Osten, E. Bugiel, and P. Zaumseil, *Appl. Phys. Lett.* 64 (25), 20 June (1994).
16. D. De Salvador, M. Petrovich, M. Berti, F. Romanato, E. Napolitani, A. Drigo, J. Stangl, S. Zerlauth, M. Mühlberger, F. Schäffler, G. Bauer, and P. C. Kelires, *Physical Review*, B Volume 61, number 19, 15 May (2000).
17. W. Windl, O. F. Sankey, and J. Menendez, *Physical Review*, B Volume 57, number 4, 15 January (1998).
18. S. Bodnar, and J. L. Regolini, *J. Vac. Sci. Technol. A* 13(5), Sep/Oct (1995).
19. J. A. Borders, S. T. Picraux, and W. Beezhold, *Appl. Phys. Lett.*, Vol. 18, No. 11, 1 June (1971).
20. J. M. Hartmann, V. Benevent, J. P. Barnes, M. Veillerot, and C. Deguet, *Semicond. Sci. Technol.* 28 025017 (2013).